A compact size coupling controllable filter with separate electric and magnetic coupling paths

Ma, Kaixue; Ma, Jianguo; Yeo, Kiat Seng; Do, Manh Anh

2006

Ma, K., Ma, J. G., Yeo, K. S., & Do, M. A. (2006). A compact size coupling controllable filter with separate electric and magnetic coupling paths. IEEE Transactions on Microwave Theory and Techniques, 54(3), 1113-1119.

https://hdl.handle.net/10356/90852

https://doi.org/10.1109/TMTT.2005.864118

A Compact Size Coupling Controllable Filter With Separate Electric and Magnetic Coupling Paths

Kaixue Ma, *Member, IEEE*, Jian-Guo Ma, *Senior Member, IEEE*, Kiat Seng Yeo, and Manh Anh Do

***Abstract*—This paper presents the characteristics of a miniaturized microstrip filter, which has two separate coupling paths: electric coupling path and magnetic coupling path between two resonators. Either magnetic coupling or electric coupling in two paths can be dominant in the total coupling coefficient of the inter-stage resonators with the similar configuration, but different positions of transmission zero points (ZPs). Based on the proposed filter topology, second- and fourth-order filters have been designed and fabricated for the first time. Advantages of using this type of filter are not only its low insertion loss and much more compact size, but also its controllable transmission ZPs.**

***Index Terms*—Bandpass filter (BPF), odd and even mode, separate electric and magnetic coupling paths (SEMCPs), zero point (ZP).**

I. Introduction

As ONE of the key components in RF front-ends, filters with compact size, good performance, and low cost are highly demanded. Planar filters have great advantages over other types as regards these aspects and, thus, draw much attention. In order to reduce the size of the planar filter without sacrificing performance, many techniques have been reported in the literature (e.g., see [1]–[13]). For instance, instead of using a dual-mode half-wavelength resonator [1]–[4] or ring resonator [5]–[7], a quarter-wavelength resonator has been used [9]–[13], which can also provide a wider stopband.

It is desirable to design a filters in which extra transmission zero points (ZPs) can be generated without sacrificing the passband response [8], [13], [14]. For example, the extra ZPs of the filter can be adjusted to reject possible interferences and to improve stopband rejection. Thus, a low-order filter with the help of extra ZPs can meet the stopband requirements that are usually achieved by high-order filters. It is also known that the lower order filters generally have smaller sizes and lower insertion loss compared with the high-order filters. To generate more expected ZPs, the coupling mechanism must be investigated clearly. There are many papers in the literature that have paid attention to the coupling mechanism. Source–load coupling or cross-coupled topologies of elliptical filters are widely adopted [8], [11], [13]. The general coupling matrix is used to represent the coupling relationship for filter synthesizing [15]–[18], [21]. It can be seen that only one coupling parameter exists between any two adjacent resonators in the coupling matrix. For the inter-stage coupling of the quarter-wavelength filter, the inter-stage coupling in these reports can be classified as electric coupling, magnetic coupling, or mixed coupling (both electric and magnetic coexist, but cannot be separated in space due to distributed effects). The inter-stage coupling of most reported quarter-wavelength filters has one physical coupling path with one of these three coupling types between two adjacent resonators. The filters in [20] achieved good performances by using a suspended stripline quarter-wavelength stepped-impedance resonator (SIR) and generating additional ZPs by coexisted the electric and magnetic coupling.

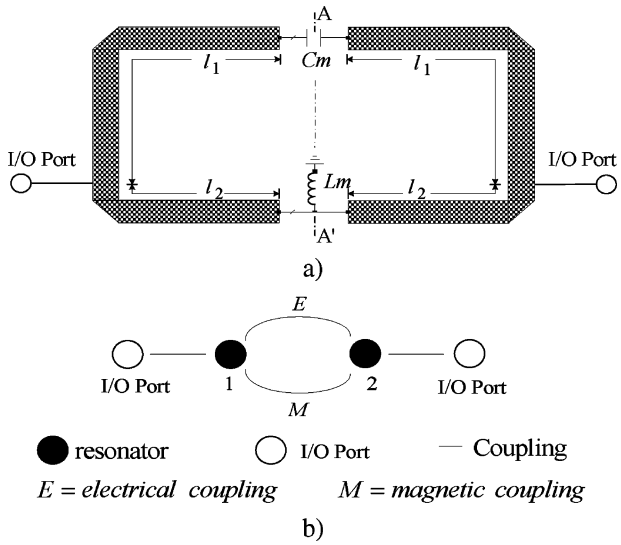

Fig. 1. Proposed second-order filter configuration and the topology. (a) Configuration with lump coupling elements. (b) Filter topology.

In this paper, a filter topology and configuration (see Fig. 1), which provide two controllable separate electric and magnetic coupling paths (SEMCPs), are proposed. The characteristics of the microstrip filters, based on the SEMCP configuration using modified uniform quarter-wavelength resonators, have been investigated theoretically and experimentally. The size reduction, frequency-dependent coupling canceling, and additional ZP generation are demonstrated. The filters, with additional ZPs in low, upper stopband, or both, corresponding to electric, magnetic, or both dominant conditions, have been designed. The general topology and configuration of high-order filter are also given.

This paper is arranged as follows. In Section II, the SEMCP configuration by using lump coupling loading and topology are introduced. Odd- and even-mode analysis is used to investigate the coupling characteristics, external quality factors and transmission responses. In Section III, second-order bandpass filters

Manuscript received July 3, 2005; revised September 18, 2005 and November 3, 2005.

K. Ma, K. S. Yeo, and M. A. Do are with the Center for Integrated Circuits and Systems, Nanyang Technological University, Singapore 635798 (e-mail: pg05296107@ntu.edu.sg).

J.-G. Ma is with the School of Electronic Engineering, University of Electronic Science and Technology of China, Chendu 610054, China.

Digital Object Identifier 10.1109/TMTT.2005.864118

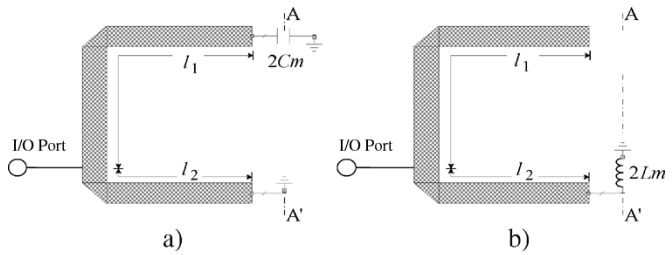

Fig. 2. Equivalent even and odd- mode configurations. (a) Even mode. (b) Odd mode.

(BPFs) with distributed SEMCPs are characterized, designed, and verified by the experiment. In Section IV, the high-order SEMCP filter topology is proposed and a fourth-order BPF with a distributed loading SEMCP is designed and fabricated. A conclusion is given in Section V.

II. Analysis of Filters With SEMCP

Fig. 1(a) shows the configuration of a second-order SEMCP filter loaded with lump coupling elements (Lm and Cm). Two sections of transmission lines are connected in series by a lump capacitor Cm, which is called an electric coupling path. Meanwhile, a lump inductor Lm is shunted along the other two ends of two transmission lines, which is called a magnetic coupling path. The coupling relationships and resonators are illustrated in the filter topology of Fig. 1(b). As in Fig. 1(a), the I/O ports and physical structure are symmetrical with respect to the reference plane AA'. An odd- and even-mode analysis [22] is adopted to analyze this structure. From the mechanism of the resonator resonance, the structure is resonant when its input admittance is zero for both the even and odd modes, i.e.,

$$Y_{\text{even}} = Y_{\text{odd}} = 0. \tag{1}$$

For the even-mode case, the equivalent-circuit representation of the resonator when the magnetic wall is applied at the AA' plane is demonstrated in Fig. 2(a). The even-mode input admittance is derived as

$$Y_{\text{even}} = jY_c\left[\tan\beta_e l_1 + \frac{2\omega_e L_m Y_c \tan\beta_e l_2 - 1}{2Y_c\omega_e L_m + \tan\beta_e l_2}\right] \tag{2}$$

where β_e is the propagation constant at the even-mode resonance angular frequency ω_e, and $Z_c = 1/Y_c$ is the characteristic impedance of the resonator.

Using (1) and (2), we have

$$\frac{2L_m\omega_e}{Z_c} = \frac{1}{\tan\beta_e(l_1+l_2)}. \tag{3}$$

For a small L_m, $l_1 + l_2 \approx \lambda_g/4$, the right-hand side of (3) can be expanded by using Taylor expansion at $l_1 + l_2 = \lambda_g/4$. By omitting the high-order terms, (3) can be written by

$$\frac{2L_m\omega_e}{Z_c} + \beta_e(l_1+l_2) = \frac{\pi}{2}. \tag{4}$$

Since

$$\beta_e = \frac{\omega_e\sqrt{\varepsilon_{re}}}{c}$$

where c is speed of the light in the free space.

The even-mode resonant angular frequency can be given by

$$\omega_e = \frac{\pi}{2(2L_mY_c + A)} \tag{5}$$

where

$$A = \frac{\sqrt{\varepsilon_{re}}(l_1+l_2)}{c}.$$

For the odd-mode case, the equivalent-circuit representation of the resonator when the electric wall is applied at the AA' plane is illustrated in Fig. 2(b). The odd-mode input admittance is

$$Y_{\text{odd}} = jY_c\left[\frac{2\omega_o C_m + Y_c\tan\beta_o l_1}{Y_c - 2\omega_o C_m\tan\beta_o l_1} - \cot\beta_o l_2\right] \tag{6}$$

where β_o is the propagation constant at the odd-mode resonance angular frequency ω_o.

Using (1) and (6), it reads

$$\frac{2C_m\omega_o}{Y_c} = \frac{1}{\tan\beta_o(l_1+l_2)}. \tag{7}$$

For a small Cm, $l_1 + l_2 \approx \lambda_g/4$, the right-hand side of (7) can be expanded by using Taylor expansion at $l_1 + l_2 = \lambda_g/4$. By omitting the high-order terms, (7) can be written as

$$\frac{2C_m\omega_o}{Y_c} + \beta_o(l_1+l_2) = \frac{\pi}{2}. \tag{8}$$

Since

$$\beta_o = \frac{\omega_o\sqrt{\varepsilon_{re}}}{c}.$$

The odd-mode resonant angular frequency can be determined by

$$\omega_o = \frac{\pi}{2(2C_mZ_c + A)}. \tag{9}$$

The center frequency of the BPF can be approximated by averaging the even- and odd-mode frequencies as

$$f_0 = \frac{1}{4\pi}(\omega_e+\omega_o) = \frac{1}{8}\left[\frac{1}{2C_mZ_c+A} + \frac{1}{2Y_cL_m+A}\right]. \tag{10}$$

The coupling between two modes is characterized by the coupling coefficient C [7], which can be computed from the knowledge of even- and odd-mode frequencies as

$$C = \frac{\omega_o^2-\omega_e^2}{\omega_o^2+\omega_e^2} = F(Y_cL_m - C_mZ_c) = M - E \tag{11}$$

where

$$F = \frac{4(A + Y_cL_m + Z_cC_m)}{(2Y_cL_m + A)^2 + (2Z_cC_m + A)^2}$$

$$M = FY_cL_m$$

and

$$E = FZ_cC_m\,.$$

From (11), the inter-stage couplings of the SEMCP are formed by two separate parts, i.e., electric (E) coupling and magnetic (M) coupling, as illustrated in the filter topology of Fig. 1(b). The couplings in two coupling paths are dependent and have the canceling effects for the total coupling coefficient C.

The external quality factor [23] can be determined by averaging the external quality factor of the even and odd modes

$$Q_e = \frac{1}{2}(Q_{e,e} + Q_{e,o}) = \frac{\pi}{4}\frac{Z_L}{Z_c}\left(\frac{1}{\sin^2\left(\beta_e(l_2+l_e)\right)} + \frac{1}{\sin^2\beta_o(l_2)}\right) \quad (12)$$

where

$$l_e = \frac{2Y_cL_mc}{\sqrt{\varepsilon_{re}}}.$$

$Z_L = 1/Y_L$ is the impedance at the I/O ports.

The transmission characteristic of the filter can be calculated from the odd- and even-mode input admittances [9] and is expressed as

$$S_{21} = \frac{\overline{Y}_{\text{odd}} - \overline{Y}_{\text{even}}}{\left(1+\overline{Y}_{\text{odd}}\right)\left(1+\overline{Y}_{\text{even}}\right)} \quad (13)$$

where $\overline{Y}_{\text{even}} = Y_{\text{even}}/Y_L$ and $\overline{Y}_{\text{odd}} = Y_{\text{odd}}/Y_L$ are normalized even- and odd-mode admittances, respectively. MATLAB6.5 is used to discuss the following two useful conditions.

- *Magnetic coupling M dominant* $(C > 0)$

  Now $Y_cL_m > C_mZ_c$, the operating frequency of the odd mode is higher than that of the even mode and the coupling in the bottom coupling path of Fig. 1(a) is dominant. For the same dimension of the transmission line and I/O ports, the effects of coupling elements (L_m and C_m) in two coupling paths on filter performance are compared in Fig. 3. When $C_m = 0$, there is only one ZP generated in the high stopband due to the harmonic effects. While $Cm > 0$, there is an additional ZP generated in the high stopband and the filter demonstrates a good rolloff in the high stopband. If both L_m and C_m are increased, the operating frequency can be shifted down while keeping the coupling coefficient fixed. However, the rejection in stopband will be reduced. When Lm is fixed at $L_m = 0.15$ nH, the increased C_m (see $C_m = 0$ pF and $C_m = 0.01$ pF) can decrease the bandwidth of the filter by reducing the operating frequency of the odd mode.
- *Electric coupling E dominant* $(C < 0)$

  Now $Y_cL_m < C_mZ_c$, the operating frequency of the even mode is higher than that of the odd mode and the coupling in the upper coupling path of Fig. 1(a) is dominant. For the same dimension of the transmission line and I/O ports, the effects of coupling elements (L_m and C_m) in two coupling paths on filter performances are compared in Fig. 4. When $L_m = 0$, no finite ZP can be generated in the stopband. When $L_m > 0$, there are two additional ZPs generated in the stopband and the filter demonstrates a good rolloff. When both L_m and C_m are increased, the operating frequency can be shifted down, while keeping the coupling coefficient fixed. However, the rejection in the stopband will be reduced. When C_m is fixed at $C_m = 0.05$ pF, the increased L_m (see $L_m = 0.0$ nH and $L_m = 0.05$ nH) can decrease the bandwidth of the filter by reducing the coupling coefficient C or the operating frequency of the even mode.

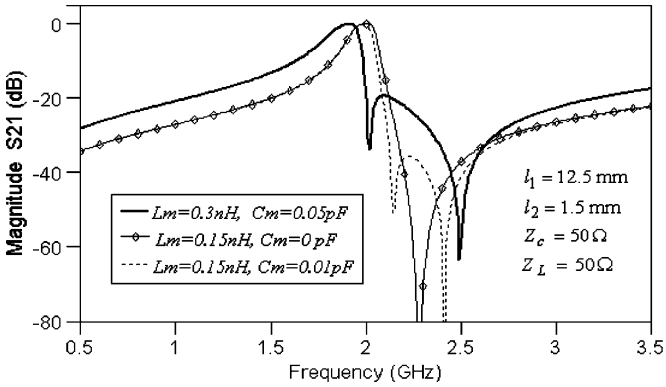

Fig. 3. Spectrum responses of M dominant SEMCP filters.

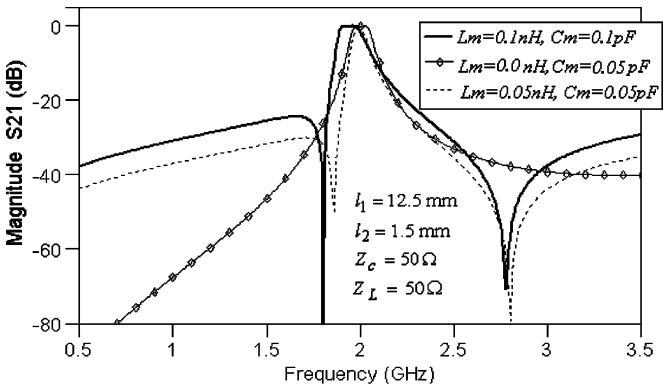

Fig. 4. Spectrum responses of E dominant SEMCP filters.

By comparing Fig. 3 with Fig. 4, it is interesting to note that, for the E and M dominant SEMCP filters with the same transmission line dimensions (the same width of W_0 and length of l_1 and l_2), the filter response can be completely controlled by choosing a different dominant coupling path, as well as different coupling element values. The canceling effects of E and M couplings in two paths are helpful for a narrow bandwidth filter, where a smaller coupling coefficient is required [10]. One additional ZP, generated in either the low or upper stopband, can be used to improve the stopband performance.

III. Second-Order Filter Realization

For more general applications, the lump capacitor can be implemented by a coupled gap or coupled transmission lines and the lump inductance can be realized by a via-hole [24], [25] or a section of a high characteristic impedance transmission line connected to the ground through a via-hole in series [10]. In Fig. 5, the three configurations for second-order SEMCP filters with a tap feeder are illustrated. The filter topology is shown in Fig. 1(b). Fig. 5(i) illustrates the structure when there exists a weak electric coupling, generated by the coupling gap, and a magnetic coupling, generated by the common via ground. Fig. 5(ii) shows the case when both electric coupling, generated by parallel coupling lines with the length of l_J, and magnetic coupling, generated by a section of high characteristic impedance transmission line (with length of l_h and width of w_h) connected to the ground through a via-hole in series, are

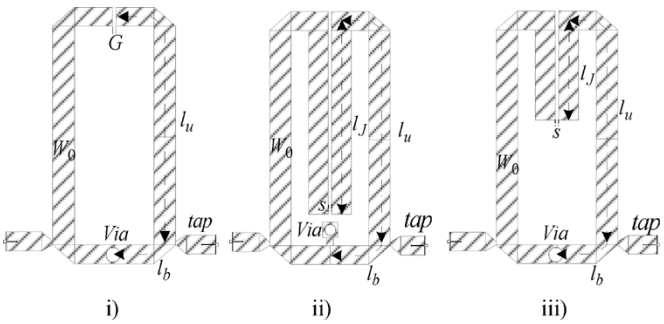

Fig. 5. Configurations of the second-order SEMCP filters. (i) Structure 1. (ii) Structure 2. (iii) Structure 3.

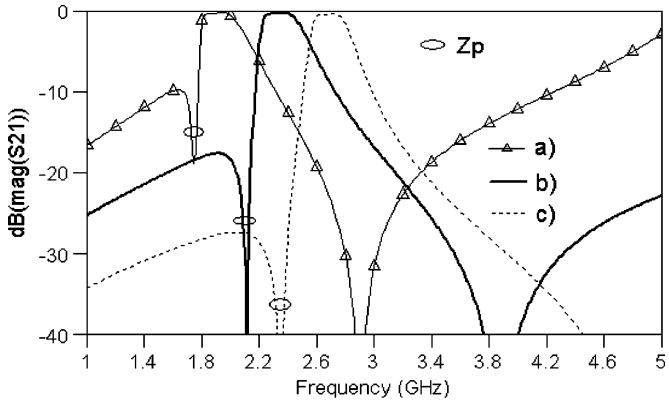

Fig. 6. Frequency responses of the second-order E dominant SEMCP filters. (a) Configuration of Fig. 5(ii) $l_b = 1.5$ mm, $l_u = 8.1$ mm; $l_J = 6.2$ mm Rvia $= 0.1$ mm $S = 0.1$ mm, $l_h = 0.4$ mm, $w_h = 0.2$ mm. (b) Configuration of Fig. 5(iii) $l_b = 1.5$ mm, $l_u = 8.1$ mm; $l_J = 3.2$ mm Rvia $= 0.1$ mm $S = 0.1$ mm. (c) Configuration of Fig. 5(iii) $l_b = 1.5$ mm, $l_u = 8.1$ mm; $l_J = 1.7$ mm, Rvia $= 0.3$ mm.

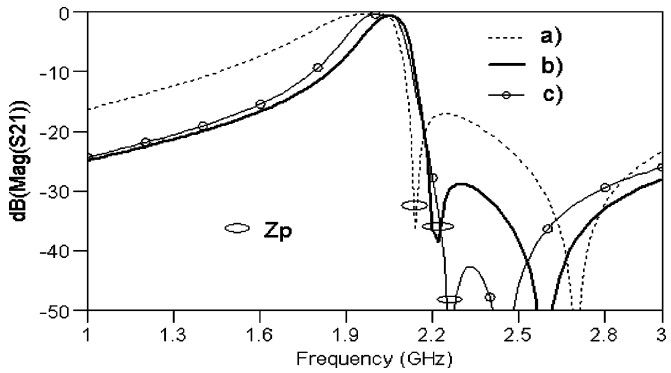

Fig. 7. Frequency response of the second-order M dominant SEMCP filters. (a) Configuration of Fig. 5(ii) $l_b = 1.5$ mm, $l_u = 11.9$ mm; $l_J = 1.15$ mm Rvia $= 0.1$ mm $S = 0.1$ mm, $l_h = 0.4$ mm, $w_h = 0.2$ mm. (b) Configuration of Fig. 5(iii) $l_b = 1.5$ mm, $l_u = 11.9$ mm; $l_J = 0.5$ mm Rvia $= 0.1$ mm $S = 0.1$ mm. (c) Configuration of Fig. 5(i) $l_b = 1.5$ mm, $l_u = 12.3$ mm; $G = 0.1$ mm, Rvia $= 0.1$ mm.

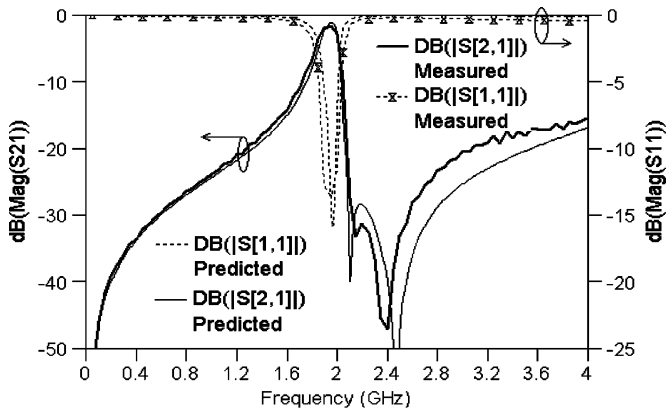

Fig. 8. Comparison of simulated and measured results of the second-order M dominant SEMCP filter.

increased as compared to Fig. 5(i). By properly choosing the dimensions of the coupling parts, either magnetic or electric coupling can be dominant. Fig. 5(iii) presents the structure where parallel coupling lines and a via ground are used. The RT/Duroid 6010 dielectric substrate with relative permittivity of $\varepsilon_r = 10.2$ and thickness of 0.635 mm and commercial EM software IE3D 9.0 are used in the following design and analysis. Fig. 6 demonstrates the conditions when the electric coupling is dominant. The length of l_u, which mainly determines the occupied area of the filter, is fixed. As expected, similar characteristics as the lump-element condition in Section II can be achieved. When the external quality factor is fixed, the increased magnetic and electric couplings cancel each other in the operating frequency range. Thus, the filter bandwidth, which is mainly determined by the inter-stage coupling coefficient C, changes very little, while the operating frequency is shifted down due to the increased loadings in two coupling paths. Fig. 7 gives the condition when magnetic coupling is dominant. The length of each resonator is fixed, and the filter of the SEMCP can generate additional ZP in the upper rejection band. The increased E and M couplings are also canceled by each other. Thus, the filter bandwidth can be maintained even when the electric and magnetic couplings are increased; while the operating frequency is shifted down by increased coupling in each path due to the loading effects in two coupling paths. In Fig. 8, results of a magnetic coupling dominant filter in Fig. 5(i) are compared. There are two finite transmission ZPs generated in the upper stopband. The first ZP, close to the operating frequency, is generated by canceling effects of the electric and magnetic coupling, and the generation of the second ZP is mainly due to the harmonic effects of the distributed transmission line [13].

In Fig. 9, simulated and measured results of the electric coupling dominant filter in Fig. 5(iii) are compared. The discrepancies in bandwidth and attenuation in low stopband between the measurement and simulation may come from the differences between the simulated and measured structure [20], which includes the fabrication errors in the single via ground and narrow coupling gap. The measured specifications of the filter are: 1) operating frequency of 2.4 GHz; 2) 1-dB bandwidth of 380 MHz; 3) the insertion loss of 0.85 dB; and 4) the occupied area (without considering the I/O feed lines) is only $0.065\lambda_0 \times 0.027\lambda_0$ (λ_0 is the free-space wavelength at operating frequency). The fabricated photograph of the second-order filters are illustrated in Fig. 10.

IV. High-Order SEMCP Filter

Fig. 11 demonstrates an nth-order SEMCP filter topology by using the SEMCP topology. The main differences of SEMCP fil-

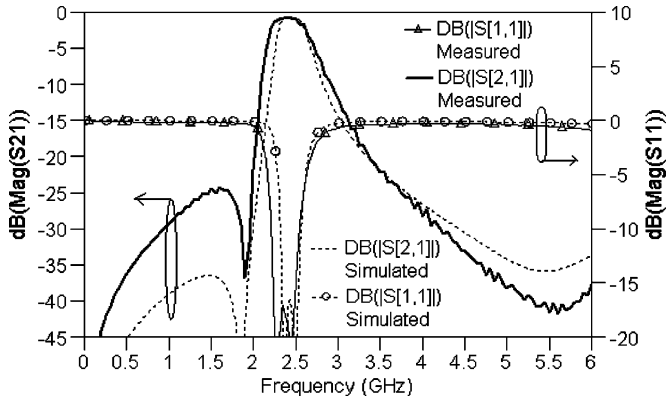

Fig. 9. Comparison of simulated and measured results of the second-order E dominant SEMCP filter.

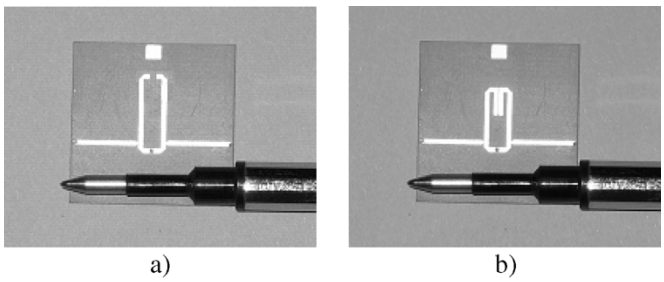

Fig. 10. Fabricated second-order SEMCP filter. (a) M dominant. (b) E dominant.

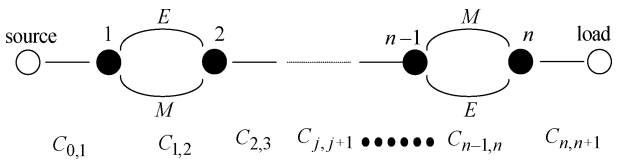

Fig. 11. Topology of the high-order SEMCP filter.

ters from filters in [15]–[18] are that two separate controllable E and M coupling paths exist between some adjacent resonators in the filter. The general filter coupling topology in these papers has only one coupling path in any two adjacent resonators. The filter structures and equivalent topologies are also different from that of references [19]–[21]. In the SEMCP filter topology, the SEMCPs exist in interval, and the inter-stage coupling coefficient in SEMCP structures with complicated distributed E and M couplings can be determined using the full-wave EM determined procedure [9]. The dominant electric coupling can be set in order to generate ZPs in the low stopband, while the dominant magnetic coupling can be used to generate ZPs in the upper stopband. If the filter has both dominant E and M SEMCPs simultaneously, it is believed that the ZPs can be generated in the lower and upper stopband simultaneously.

The configuration and topology of a fourth-order SEMCP filter are shown in Fig. 12(a) and (b), respectively. Two E dominant SEMCPs are introduced between resonators 1 and 2 as well as 3 and 4. Firstly, a filter with 17% fractional bandwidth (FBW) is designed. The total coupling coefficient C is the result of coupling after E and M canceling [refer to (11)].

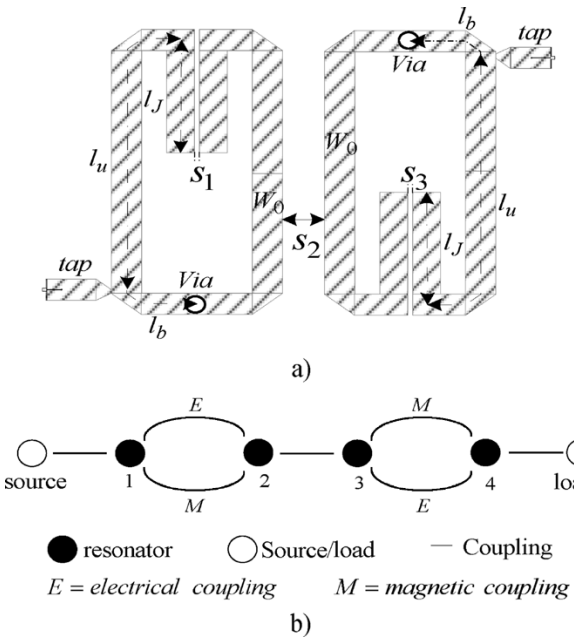

Fig. 12. Configuration and topology of the fourth-order SEMCP filter. (a) Configuration. (b) Topology.

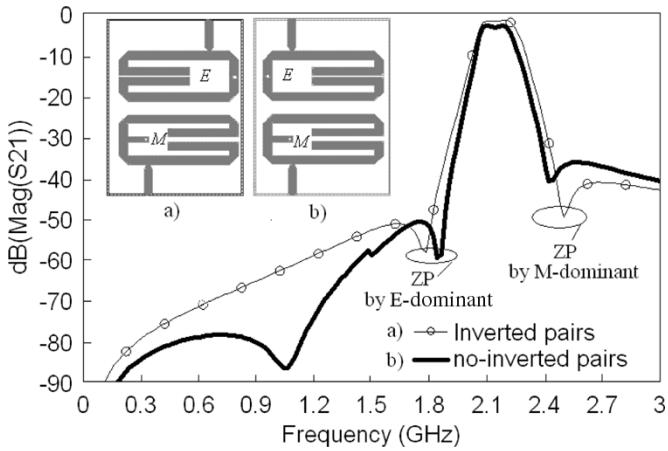

Fig. 13. Configuration and simulation of the fourth-order E and M dominant SEMCP filter. Dimension [for both structures (a) and (b)]: $W_0 = 0.59$ mm, $l_b = 2.9$ mm, $l_u = 5.94$ mm, $l_J = 4.52$ mm $R_{\rm via} = 0.1$ mm, $S_1 = 0.13$ mm, $S_2 = 0.9$ mm, $S_2 = 0.3$ mm, $l_h = 1.2$ mm, $w_h = 0.4$ mm (refer to Figs. 5 and 112).

The external quality factor Q_e and the inter-stage coupling C can be calculated from [9] and [10], and are $Q_e = 6.52$ and

$$\overline{C} = \begin{bmatrix} 0 & -0.141 & 0 & 0 \\ -0.141 & 0 & 0.112 & 0 \\ 0 & 0.112 & 0 & -0.141 \\ 0 & 0 & -0.141 & 0 \end{bmatrix}$$

where the negative signs of coupling coefficients in the coupling matrix $\overline{C}$ denote the electric coupling, as in (11). The optimized filter dimensions are $W_0 = 0.59$ mm, $l_b = 3.95$ mm, $l_u = 5.94$ mm, $l_J = 4.52$ mm, $S_1 = S_3 = 0.09$ mm, $R_{\rm via} = 0.2$ mm, and $S_2 = 0.6$ mm. To demonstrate the control of the ZPs both in the low and high stopband, the configurations and EM simulation results of the fourth-order SEMCP filters with one E dominant pair and one M dominant pair are shown in Fig. 13. Filters with inverted pairs and no-inverted SEMCP pairs have the same dimensions. Each filter generates additional

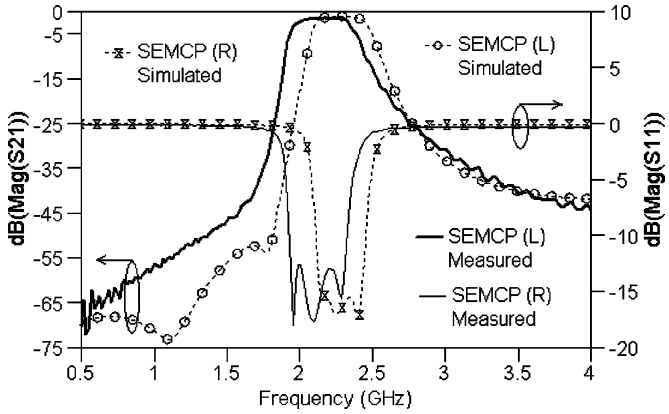

Fig. 14. Results of the fourth-order E dominant SEMCP filter.

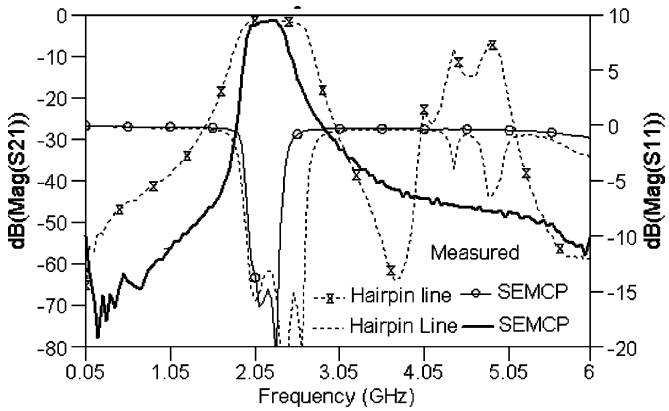

Fig. 15. Comparison of measured results of the fourth-order E dominant SEMCP filter and fourth-order hairpin filter.

ZPs in both the lower and upper stopbands, as compared to a traditional combline filter. One more ZP, generated in the lower stopband of on-inverted SEMCP pairs is mainly because of the inter-stage coupling between the E and M dominant SEMCP pairs. The results of simulation and the experiment of the filter in Fig. 12 are shown in Figs. 14 and 15. Fig. 14 shows the results in the frequency range of 0.5∼4 GHz. The rejection at 1.97 GHz (−3-dB edge of the filter in the lower sideband) is −3 dB, while the rejection at 1.7 GHz (0.63 BW) is better than −40 dB. In Fig. 14, there are two ZPs (1.77 GHz with rejection of −53.8 dB and 1.11 GHz with rejection of −73.2 dB) in the lower stopband of the simulation. The discrepancies between simulation and measurement may come from differences between simulated and realized structure. The ZPs may be shifted toward the lower frequency range and be buried in the noise floor in measurement. A fourth-order hairpin line filter with a bandwidth of $\mathrm{BW} = 760$ MHz $(\mathrm{FBW} = 34\%)$ has also been designed and fabricated as a contrast to the SEMCP filter. The measured results of the fourth-order SEMCP filter and fourth-order hairpin line filter are compared in Fig. 15. The measured minimum insertion losses for the SEMCP and hairpin line filters are 1.4 and 1.48 dB, respectively. The rolloff of the SEMCP filter in the low stopband is much steeper than that of the hairpin line filter. To reduce the bandwidth of the hairpin line filter, the spaces between the adjacent resonators should be further increased, and this may lead to an increase in the filter size [26]. It can be seen that the filter with the SEMCP has the advantages

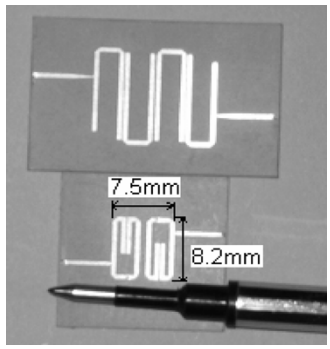

Fig. 16. Fourth-order SEMCP and hairpin filters.

of controlling the ZPs and inter-stage coupling and the possibility of achieving low insertion loss and compact size simultaneously. The photographs of an SEMCP filter and hairpin line filter are shown in Fig. 16. The size of the fabricated fourth-order SEMCP filter occupies an area as small as $0.06\lambda_0 \times 0.0545\lambda_0$ $(0.82\ \mathrm{cm} \times 0.75\ \mathrm{cm} = 0.615\ \mathrm{cm}^2)$, which is only one-third of that of the fabricated hairpin line filter (without considering the I/O feed lines, $1.26\ \mathrm{cm} \times 1.48\ \mathrm{cm} = 1.865\ \mathrm{cm}^2$).

V. Conclusion

In this paper, a novel SEMCP filter topology together with a configuration has been proposed. The characteristics of the E dominant and M dominant SEMCP filters have been investigated and the advantages such as compact size, sharp rolloff, and low loss have been demonstrated via simulation and experiment. The general high-order SEMCP filter topology has been introduced and the fourth-order E dominant filter with compact size and low insertion loss has been implemented. It should be noted that, although the topology has been realized by using a microstrip line, it may be applicable to other transmission lines such as the coplanar waveguide (CPW) stripline. For example, if the CPW transmission line is used to realize the filter topology, the grounding via-hole can be replaced by a ground shunt.

Acknowledgment

The authors thank K. T. Chan, MEDs Technologies Pte. Ltd., Singapore, for help with fabrication. The authors further thank the editor and reviewers for their thoughtful comments and suggestions.

References

[1] S. B. Cohn, "Parallel-coupled transmission-line resonator filters," *IRE Trans. Microw. Theory Tech.*, vol. MTT-6, no. 4, pp. 223–231, Apr. 1958.

[2] E. G. Cristal and S. Frankel, "Hairpin-line and hybrid hairpin-line half-wave parallel-coupled-line filters," *IEEE Trans. Microw. Theory Tech.*, vol. MTT-20, no. 11, pp. 719–728, Nov. 1972.

[3] M. Sagawa, K. Takahashi, and M. Makimoto, "Miniaturized hairpin resonator filters and their application to receiver front-end MIC's," *IEEE Trans. Microw. Theory Tech.*, vol. 37, no. 12, pp. 1991–1996, Dec. 1989.

[4] H.-K. Zeng, A. Hsiao, W.-H. Hsu, S.-W. Wu, J.-Y. Lin, K.-H. Wu, J.-Y. Juang, T.-M. Uen, Y.-S. Gou, and J.-T. Kuo, "Miniaturized 3 GHz cross-coupled planar microwave filters," *IEEE Trans. Microw. Theory Tech.*, vol. 14, no. 3, pp. 107–111, Mar. 2004.

[5] I. Wolff, "Microstrip bandpass filter using degenerate modes of microstrip ring resonator," *Electron. Lett.*, vol. 8, no. 12, pp. 779–781, Jun. 1972.

[6] L. Zhu and K. Wu, "A joint field/circuit design model of microstrip ring dual-mode filters: Theory and experiments," in *Proc. Asia–Pacific Microwave Conf.*, 1997, pp. 865–868.

[7] I. Awai, A. C. Kundu, and T. Yamashita, "Equivalent-circuit representation and explanation of attenuation poles of a dual-mode dielectric-resonator bandpass filter," *IEEE Trans. Microw. Theory Tech.*, vol. 46, no. 12, pp. 2159–2163, Dec. 1998.
[8] C.-H. Wang, Y.-S. Lin, and C. H. Chen, "Novel inductance-incorporated microstrip coupled-line bandpass filters with two attenuation poles," in *IEEE MTT-S Int. Microw. Symp. Dig.*, 2004, pp. 1979–1982.
[9] J.-S. Hong and M. J. Lancaster, *Microstrip Filters for RF/Microwave Applications*. New York: Wiley, 2001.
[10] G. L. Matthaei, L. Young, and E. M. T. Jones, *Microwave Filters, Impedance-Matching Networks, and Coupling Structures*. Dedham, MA: Artech House, 1964.
[11] J. Zhou, M. J. Lancaster, and F. Huang, "Coplanar quarter-wavelength quasi-elliptic filters without bond-wire bridges," *IEEE Trans. Microw. Theory Tech.*, vol. 52, no. 4, pp. 1150–1156, Apr. 2002.
[12] T. Kitamura, Y. Horii, M. Geshiro, and S. Sawa, "A dual-plane comb-line filter having plural attenuation poles," *IEEE Trans. Microw. Theory Tech.*, vol. 50, no. 4, pp. 1216–1219, Apr. 2004.
[13] K. Ma, J.-G. Ma, M. A. Do, and K. S. Yeo, "A novel compact two-order band pass filter with three zero points," *Electron. Lett.*, vol. 41, pp. 846–848, Jul. 2005.
[14] J. L. Li, J. X. Chen, J. P. Wang, W. Shao, Q. Xue, and L. J. Xue, "Miniaturised microstrip bandpass filter using stepped impedance ring resonators," *Electron. Lett.*, vol. 40, no. 22, pp. 1420–1421, 2004.
[15] R. J. Cameron, "Advanced coupling matrix synthesis techniques for microwave filters," *IEEE Trans. Microw. Theory Tech.*, vol. 51, no. 1, pp. 1–10, Jan. 2003.
[16] U. Rosenberg and S. Amari, "Novel coupling schemes for microwave resonator filters," *IEEE Trans. Microw. Theory Tech.*, vol. 50, no. 12, pp. 2896–2902, Dec. 2002.
[17] J.-R. Qian and W.-C. Zhuang, "New narrow-band dual-mode bandstop waveguide filters," *IEEE Trans. Microw. Theory Tech.*, vol. 31, no. 12, pp. 1045–1050, Dec. 2003.
[18] R. Lavy, "New cascaded trisections with resonant cross-couplings (CTR sections) applied to the design of optimal filters," in *IEEE MTT-S Int. Microw. Symp. Dig.*, 2004, pp. 447–450.
[19] S. Amari and J. Bornemann, "Using frequency-dependent coupling to generate finite attenuation poles in direct-coupled resonator bandpass filters," *IEEE Microw. Guided Wave Lett.*, vol. 9, no. 10, pp. 404–406, Oct. 1999.
[20] W. Menzel and M. Berry, "Quasilumped suspended stripline filters with adjustable transmission zeroes," in *IEEE MTT-S Int. Microw. Symp. Dig.*, 2004, pp. 1601–1604.
[21] W. C. Tang, J. Frenna, and D. Siu, "Odd order elliptic waveguide cavity filters," U.S. Patent 4 644 305, Feb. 17, 1987.
[22] I. C. Hunter, *Theory and Design of Microwave Filters*. London, U.K.: IEE Press, 2001.
[23] J. S. Wong, "Microstrip tapped-line filter design," *IEEE Trans. Microw. Theory Tech.*, vol. MTT-27, no. 1, pp. 44–50, Jan. 1979.
[24] M. E. Goldfarb and R. A. Pucel, "Modeling via hole grounds in microstrip," *IEEE Microw. Guided Wave Lett.*, vol. 1, no. 6, pp. 135–137, Jun. 1991.
[25] D. G. Swanson, "Grounding microstrip lines with voles," *IEEE Trans. Microw. Theory Tech.*, vol. 40, no. 8, pp. 1719–1721, Aug. 1992.
[26] G. L. Matthaei, "Narrow-band, fixed-tuned, and tunable bandpass filter with zig–zag hairpin-comb resonators," *IEEE Trans. Microw. Theory Tech.*, vol. 51, no. 4, pp. 1214–1219, Apr. 2003.

Kaixue Ma (S'05–M'05) received the B.E. and M.E. degrees in electronics engineering from Northwestern Polytechnical University (NWPU), Xi'an, China, in 1997 and 2001 respectively, and currently working toward Ph.D. degree in electrical and electronic engineering with Nanyang Technological University, Singapore.

From 1997 to 2002, he was with the 504th Research Institute of China Academy of Space Technology (CAST), where he was a Deputy Director of the Millimeter-Wave Group involved in the design of space RF, microwave, and millimeter-wave active components and subsystem for transponder systems. He is currently with the School of Electrical and Electronic Engineering, Nanyang Technological University. He is currently focused on designing and modeling passive RF integrated circuits (ICs) on CMOS, microelectromechanical systems (MEMS), and printed circuit board (PCB) processes.

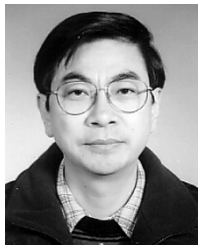

Jian-Guo Ma (M'96–SM'97) received the B.Sc. and M.Sc. degrees (with honors) from Lanzhou University, Lanzhou, China, in 1982 and 1988, respectively, and the Doctoral degree in engineering from Gerhard–Mercator University, Duisburg, Germany, in 1996.

From January 1982 to March 1991, he was with Lanzhou University, where he was involved with RF and microwave engineering. Prior to joining Nanyang Technological University, Singapore, in 1997, he was with the Technical University of Nova Scotia, Halifax, NS, Canada. He was an Associate Professor and Director of the Center for Integrated Circuits and Systems, Nanyang Technological University of Singapore. Since 2005, he has been with the University of Electronic Science and Technology of China (UESTC), Chendu, China. He has authored or coauthored over 180 technical papers and two books. He holds six patents in CMOS RF integrated circuits (RFICs). His research interests are RF integrated-circuit RFIC designs for wireless applications, RF characterization and modeling of semiconductor devices, RF interconnects and packaging, system-on-chip (SOC) applications, electromagnetic compatibility (EMC)/electromagnetic interference (EMI) in RFICs, and monolithic-microwave integrated-circuit (MMIC) applications.

Kiat Seng Yeo received the B.E. degree (with honors) and Ph.D. degree from Nanyang Technological University, Singapore, in 1993 and 1996, respectively, both in electrical engineering.

In 1996, he joined the School of Electrical and Electronic Engineering, Nanyang Technological University, as a member of the academic staff. He is currently the Head of the Division of Circuits and Systems, Nanyang Technological University. He provides consulting to statutory boards and multinational corporations in the areas of semiconductor devices and integrated circuit design. His research interests include device characterization and modeling, RFIC design, and low-voltage low-power IC design.

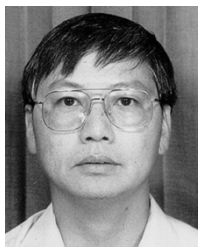

Manh Anh Do received the B.E. (with honors) in electronics and Ph.D. degree in electrical engineering from the University of Canterbury, Canterbury, New Zealand, in 1973 and 1977, respectively.

From 1977 to 1989, he held various positions including Research and Development Engineer and Production Manager with Radio Engineering Ltd., Research Scientist with the Fisheries Research Centre, Canterbury, New Zealand, and Senior Lecturer with the National University of Singapore. In 1989, he joined the School of Electrical and Electronic Engineering, Nanyang Technological University (NTU), Singapore, as a Senior Lecturer, and became an Associate Professor in 1996 and Professor in 2001. He has been a consultant for numerous projects in the Singapore electronic industry and was the principal consultant for the design, testing, and implementation of the $200 000 000 electronic road pricing (ERP) island-wide project in Singapore (1990–2001). Since 1995, he has been Head of the Division of Circuits and Systems, School of Electrical and Electronic Engineering, NTU. He has authored or coauthored over 150 papers in the areas of electronic and communication circuits and systems. His current research concerns digital and mobile communications, RFIC design, mixed-signal circuits, and intelligent transport systems. He has specialized in sonar designing, biomedical engineering, and signal processing.

Dr. Do is a Chartered Engineer in the U.K. and a Professional Engineer in Singapore. He is a Fellow of the Institution of Electrical Engineers (IEE), U.K. He was a council member of the IEE from 2001 to 2004. He is an associate editor for the IEEE TRANSACTIONS ON MICROWAVE THEORY AND TECHNIQUES (April 2005–March 2008).